Available online at www.sciencedirect.com

ScienceDirect

Advances in Space Research 56 (2015) 634–647

ADVANCES IN SPACE RESEARCH (a COSPAR publication)

www.elsevier.com/locate/asr

# Retrieving real-time precise co-seismic displacements with a standalone single-frequency GPS receiver

Kejie Chen *, Maorong Ge, Xingxing Li, Andrey Babeyko, Markus Ramatschi, Markus Bradke

*German Research Centre for Geosciences (GFZ), Telegrafenberg, 14473 Potsdam, Germany*

Received 28 November 2014; received in revised form 23 April 2015; accepted 24 April 2015
Available online 4 May 2015

**Abstract**

Nowadays, Global Positioning System (GPS) plays an increasingly important role in retrieving real-time precise co-seismic displacements for geo-hazard monitoring and early warning. Several real-time positioning approaches have been demonstrated for such purpose, such as real-time kinematic relative positioning, precise point positioning, etc., where dual-frequency geodetic receivers are applied for the removal of ionosphere delays by inter-frequency combination. At the same time, it would be also useful to develop efficient algorithms for estimating precise displacements with low-cost GPS receivers since they can make a denser network or multi-sensors combination without putting too much financial burden. In this contribution, we present a new method to retrieve precise co-seismic displacements in real-time using a standalone single-frequency receiver. In the new method, observations prior to an earthquake are utilized to establish a precise ionospheric delay prediction model, so that precise co-seismic displacements can be obtained without any convergence process. Our method was validated with an outdoor experiment as well as by re-processing of 1-Hz GPS data collected by the GEONET network during the 2011 Tohoku Mw 9.0 earthquake. For the latter, RMS against dual-frequency receivers constituted 2 cm for horizontal components and 3 cm for the vertical component.

We specially address the observation biases and their impact on the accuracy of single frequency positioning. Our approach makes real-time GPS displacement monitoring with dense network much more affordable in terms of financial costs.


*Keywords:* GPS; Single-frequency receiver; Ionospheric delay correction; Co-seismic displacements

## 1. Introduction

Besides monitoring secular deformation, like plate motion (see, e.g., Wang et al., 2001; Prawirodirdjo and Bock 2004; Lifton et al., 2013), GPS is also applied to detect instantaneous ground shaking in real-time for geo-hazard monitoring and early warning, for example, earthquake and tsunami early warning (see, e.g., Blewitt et al., 2006; Sobolev et al., 2007; Li et al.,2013a; Geng et al., 2013). Several positioning approaches have been proposed to capture ground displacements, such as Real Time Kinematic (RTK) relative positioning (see, e.g., Ren et al., 2010; Ohta et al., 2012; Sudhakar et al., 2013), Precise Point Positioning (PPP) (see, e.g., Larson et al., 2003; Shi et al., 2010; Li et al., 2013a). Since by relative positioning reference stations may be subjected to the earthquake shaking as well, reliability of the derived co-seismic displacements may become degraded (Ohta et al., 2012). In PPP, precise positioning is achieved based on precise orbit and clock corrections estimated from a global reference network. As no or only few stations are

* Corresponding author.
*E-mail address:* kejie@gfz-potsdam.de (K. Chen).

http://dx.doi.org/10.1016/j.asr.2015.04.029
0273-1177/

displaced by the earthquake, orbits and clocks are hardly contaminated and so is the estimated displacement. More important is that the Real-Time Service (RTS) (http://rts.igs.org/products) of the International GNSS Services (IGS) has been providing precise orbits and clocks operationally since last year, which enables real-time PPP for such applications. However, real-time PPP needs a long period (about 30 min, Geng et al., 2011) to resolve integer phase ambiguities to achieve centimeter-level accuracy. If an earthquake happens during PPP's (re) convergence period or there are data interruptions caused by an earthquake, reliability of PPP-based displacements would be significantly reduced.

In fact, a major role of GPS in applications like tsunami early warning is providing co-seismic ground displacements for subsequent tsunami source inversion. Thus, most important in this context are not absolute positions of GPS stations but their co-seismic displacements caused by an earthquake, i.e., station displacements with respect to their positions before an earthquake (Li et al., 2013b). Under this circumstance, the "variometric" approach (Colosimo et al., 2011) and temporal point positioning (TPP) (Li et al., 2013b) were proposed to avoid the long convergence of PPP solution. Furthermore, it has been proved that these methods can be equivalent if all error components are carefully considered (Li et al., 2014b).

Sobolev et al. (2007) numerically analyzed the performance of a hypothetical GPS-network on Sumatra, Indonesia, and concluded that real-time GPS-precision on the order of few centimeters is required to assure reliable GPS-based tsunami early warning. This requirement of high precision suggests dual-frequency GPS-receivers as first candidates for retrieving co-seismic displacements. On the other hand, inversion for source parameters requires, in addition to accuracy of individual displacements, a dense and geographically broadly distributed GPS-network which may comprise several hundreds of individual stations (e.g., GEONET GPS-network in Japan). The employment of a large number of expensive dual-frequency receivers makes dense GPS networks difficult to afford, especially for hazard-prone developing countries. Compared with dual-frequency receivers, single-frequency ones are not only cost-efficient, but also require lower power consumption. The later one is also very crucial for stations without regular electricity supply.

Certainly, single-frequency receivers cannot compete in accuracy of absolute positioning with dual-frequency devices. The main idea behind the current study is to employ single-frequency receivers to retrieve accurate co-seismic displacements during a very limited time interval: just 3–5 min after an earthquake. In other words, we are interested in a cost-efficient technique that can precisely derive short-term station displacements. These time considerations come from the fact that duration of local slip, that establishes significant co-seismic offset at near-field GPS stations, typically, does not exceed two to three minutes in case of tsunamigenic earthquakes. Even in the case of extremely long Giant December 2004 Sumatra–Andaman Mw > 9.1 earthquake which lasted for more than 10 min, local fast-slip rise time was under 5 min (Lay et al., 2005). Moreover, it is clear that giant (Mw > 9) subduction zone earthquakes possess enormous tsunamigenic potential and, without any doubt, must trigger tsunami warning. Our primary goal is detection and evaluation of tsunamigenic potential of earthquakes with smaller magnitudes which do not necessarily trigger tsunamis (Mw 7.5–8.5).

In order to get accurate co-seismic displacements directly from single-frequency observation, the ionospheric delay must be precisely modeled, because it cannot be eliminated by forming the ionosphere-free inter frequency combination as for dual-frequency data. Most of the approaches developed so far to tackle ionospheric correction regularly adopt a correction model (see, e.g., Klobuchar, 1987; Schaer et al., 1996). Unfortunately, due to the lack of well distributed data and simplified mathematical representations, published models can only reach an accuracy suitable for sub-meter positioning (Van Bree and Tiberius, 2012), which is definitely not enough for co-seismic displacement monitoring.

Considering that atmospheric delays and remaining orbit and clock biases could be eliminated or mostly reduced over very short intervals such as 1 s or even shorter by epoch-to-epoch differences, the "variometric" approach proposed by Colosimo et al. (2011) could be extended to single-frequency as well (Benedetti et al., 2014; Li et al., 2014a). Promisingly, even by using the broadcast ephemeris, final velocity estimation can reach millimeter per second precision. However, one important limitation for earthquake source inversion must be noted: integration of velocities into co-seismic displacements, required for the inversion, introduces inevitable bias (Tu et al., 2013).

As it was mentioned before, we are interested in displacements which take place in just a few minutes. At the same time, ionospheric delays for each satellite are normally strongly correlated during such a short period. This fact also implies that the delays can be feasibly represented by a low-order time-dependent polynomial and, furthermore, can be predicted with an accuracy of few centimeters (Geng et al., 2010; Zhang and Li, 2012). In this study, we develop a new algorithm for retrieving real-time precise co-seismic displacements with a standalone single-frequency GPS receiver by estimating ionospheric corrections based on data before earthquake and predicting the corrections for observations afterwards.

In the following, in Sections 2 and 3 we present technological details of the new algorithm, in Section 4 some specific issues related to the new algorithm are further discussed. In Section 5 we validate it by an outdoor experiment and then it is applied to process GPS dataset recorded during the Great March 11, 2011 Tohoku Mw 9.0 earthquake.

## 2. Basic observation equations

Following the approach and notation of Li et al. (2014b), GPS measurements on a single frequency can be expressed as follows

$$l_r^s = -u_r^s \cdot x - o^s - \tau^s + \tau_r + B_r^s - I_r^s + T_r^s + \varepsilon_r^s \quad (1)$$

$$P_r^s = -u_r^s \cdot x - o^s - \tau^s + \tau_r + I_r^s + T_r^s + \varepsilon_r^s \quad (2)$$

where the superscript $s$ denotes the satellite, subscript $r$-means receiver; $l_r^s$ and $P_r^s$ are the "Observed Minus Computed" (OMC) phase and range values; $u_r^s$ denotes the unit vector from receiver $r$ to satellite $s$; $x$ denotes the vector of receiver position increments relative to a priori position $x_0$, which is used for linearization; $o^s$, $\tau^s$ and $\tau_r$ stand for satellite orbit error, clock error, receiver clock error, correspondingly; $B_r^s$ is the phase ambiguity; $I_r^s$ and $T_r^s$ are the ionosphere and troposphere delays and $\varepsilon_r^s$ is measurement noise. For precise positioning, other effects, like relativistic effects, phase center variations, phase wind up, tidal loading, should be also taken into account carefully. As range observations are much noisier than phases, they are mainly used for getting receiver clock biases instead of displacement.

Since the station position is usually precisely known for any epoch $t_n$ before an earthquake, i.e., $x(t_n)$ in Eq. (1) is zero, thus it can be rewritten as:

$$l(t_n) = -o^s(t_n) - \tau^s(t_n) + \tau_r(t_n) + B(t_n) - I(t_n) + T(t_n) + \varepsilon(t_n) \quad (3)$$

For any epoch $t_m$ after the starting time of an earthquake, we have

$$l(t_m) = -u(t_m) \cdot x(t_m) - o^s(t_m) - \tau^s(t_m) + \tau_r(t_m) + B(t_m) - I(t_m) + T(t_m) + \varepsilon(t_m) \quad (4)$$

Similar to the "variometric" (Colosimo et al., 2011) and TPP (Li et al., 2013b) approaches, differenced observations between epochs $m$ and $n$ are utilized to remove or to reduce the biases.

Normally, for GPS stations designed for co-seismic displacement monitoring the occasional loss lock of signal is extremely rare. As a result, the ambiguity is usually unchanged over the time of interest. Otherwise, the epoch-differenced observations could not contribute to the estimation (Colosimo et al., 2011; Li et al., 2014a). Subtracting (3) from (4), an epoch-differenced measurement can be formed as:

$$l(t_{m,n}) = -u(t_m) \cdot x(t_m) - o^s(t_{m,n}) + \tau_r(t_{m,n}) - \tau^s(t_{m,n}) - I(t_{m,n}) + T(t_{m,n}) + \varepsilon(t_{m,n}) \quad (5)$$

Here $t_{m,n}$ indicates the difference between epoch $m$ and epoch $n$, $x(t_m)$ is the co-seismic displacements to be estimated, and $\tau_r(t_{m,n})$ the receiver clock as unknown as well.

Thanks to the contribution from RTS, accuracy of real time orbits and clocks have been improved to about a few centimeters, their remaining biases $o^s(t_{m,n})$ and $\tau^s(t_{m,n})$ in Eq. (5) are further reduced by forming the epoch-difference and, thus, can be safely neglected.

The total slant tropospheric delay is corrected by the following empirical model (Urquhart et al., 2014)

$$T = T_{zhd} \cdot M^h + T_{zwd} \cdot M^w \quad (6)$$

where $T_{zhd}$ and $T_{zhw}$ are dry and wet part of zenith delay calculated from a mathematical model (e.g., Saastamoinen 1972), and $M^h$ and $M^w$ are corresponding mapping functions dependent on elevation angle (e.g., Boehm et al., 2006), respectively. Promisingly, these models can reach accuracy of several centimeters (Schueler, 2014). If meteorological condition does not change abruptly, the tropospheric delay will change slowly against time. As a result, the accuracy of epoch-differenced tropospheric delay $T(t_{m,n})$ can be further improved. For the residual tropospheric delays, they can be precisely treated as part of ionospheric delays, because they are rather small and elevation-angle dependent. Hence, Eq. (5) can be simplified as

$$l(t_{m,n}) = \tau_r(t_{m,n}) - u(t_m) \cdot x(t_m) - I(t_{m,n}) + \varepsilon(t_{m,n}) \quad (7)$$

Finally, the biggest obstacle for retrieving accurate co-seismic displacements with single-frequency data is quantification of ionospheric variations.

## 3. Precise modeling of ionospheric delays

Similar to Eq. (7), and assuming that the loss lock do not occur before the earthquake, epoch-difference between epoch $l$ and $n$ is formed before an earthquake can be expressed as:

$$l(t_{l,n}) = \tau_r(t_{l,n}) - I(t_{l,n}) + \varepsilon(t_{l,n}) \quad (8)$$

Within a short time period of few minutes the ionospheric delay can be represented by a low-order polynomial. However, the receiver clock bias can change rapidly, especially when using low-cost receivers. Hence, an inter-satellite difference is formed to cancel the effect of the unstable receiver clock. After applying the difference between satellite $s$ and a reference satellite $j$, we can write:

$$l^j(t_{l,n}) - l^s(t_{l,n}) = -I^j(t_{l,n}) + I^s(t_{l,n}) + \varepsilon^j(t_{l,n}) - \varepsilon^s(t_{l,n}) \quad (9)$$

For each satellite, we assume that its ionospheric delay is depicted by a linear model in time $t$:

$$I = a \cdot t + b \quad (10)$$

Then Eq. (9) can be then rewritten as:

$$l^j(t_{l,n}) - l^s(t_{l,n}) = (a_s - a_j) \cdot t + b_s - b_j + \varepsilon^j(t_{l,n}) - \varepsilon^s(t_{l,n}) \quad (11)$$

Here, the multipath effect is the dominate part of the unmodeled error sources $\varepsilon$. For a permanent station, over a short time span, its surrounding environment remain almost the same and after epoch differencing $\varepsilon$ can be greatly canceled. With a continuous dataset, a set of

observation equations of type Eq. (11) can be formed to solve for the polynomial coefficients. Due to the functional correlation between $a_s$ and $a_j$, $b_s$ and $b_j$, the resulting matrix is linearly-dependent and, instead of solving for all the four parameters, one can just estimate their differences $a_s - a_j$ and $b_s - b_j$. It is easy to prove that this does not affect the final positioning result.

First of all, for generic satellite $s$, Eq. (7) can be re-written as:

$$l^s(t_{m,n}) = -u^s(t_m)\cdot x(t_m) + \tau_r(t_{m,n}) - I^j(t_{m,n}) - (I^s(t_{m,n}) - I^j(t_{m,n})) + \varepsilon^s(t_{m,n}) \quad (12)$$

Substituting in Eq. (12) ionospheric delay difference between satellite $s$ and $j$ with their polynomial representations (Eq. (10)), we obtain for all satellites but the reference satellite $j$:

$$l^s(t_{m,n}) = -u^s(t_m)\cdot x(t_m) + \tau_r(t_{m,n}) - I^j(t_{m,n}) - ((a_s - a_j)t + b_s - b_j) + \varepsilon^s(t_{m,n}) \quad (13)$$

Similarly, for the reference satellite $j$ itself, Eq. (13) is:

$$l^j(t_{m,n}) = -u^j(t_m)\cdot x(t_m) + \tau_r(t_{m,n}) - I^j(t_{m,n}) + \varepsilon(t_{m,n}) \quad (14)$$

In Eqs. (13) and (14), one can see that for all of satellite observations, they have the common parameter $\tau_r(t_{m,n}) - I^j(t_{m,n})$, which indicates that ionospheric delays of reference satellite $j$ can be absorbed by receiver clock parameter, so that we do not need to solve for $a_s, b_s, a_j, b_j$ individually.

It was confirmed that the accuracy of predicted ionospheric delay changes is highly related to the time latency $t_{m,n}$ and the satellite elevation angle (Geng et al., 2010; Zhang and Li 2012). Observations corrected by the predicted ionospheric delay changes should be properly weighted. For example, in present study, following weighting strategy is employed:

$$P = \begin{cases} 1.0 & t \leqslant 30s \\ 2\sin(E) & 30s \leqslant t \leqslant 300s \ \& \ E \leqslant 30^\circ \\ 1.0 & 30s \leqslant t \leqslant 300s \ \& \ E > 30^\circ \end{cases} \quad (15)$$

In general, predictions over a shorter time and at higher elevations are more reliable and, hence, deserve larger weight.

## 4. Implementation remarks

From the above description, the key point for retrieving real-time co-seismic displacement is precise prediction of ionospheric delay changes which can be well handled with the proposed linear fitting model. However, there are still several other aspects which may affect final solution and, hence, deserve special consideration.

The first issue is the length of the data window prior to an earthquake used to derive coefficients of the polynomial, $a$ and $b$ (see Eq. (10)). On one hand, with a long arc of data, the prediction accuracy could be degraded due to possible variations of ionospheric delays that do not follow a polynomial form. On the other hand, too few epochs may not be enough to represent the correct trend of ionospheric delay changes. Since there is no rule of thumb for selection of an optimal time window, after a number of experimental tests we decided to use two minutes prior to earthquake. Concerning the length of the prediction window: as was explained in the introduction, the ground shaking of tsunamigenic earthquakes typically is limited to 2–3 min. Having this in mind, we confine our prediction time window to five minutes.

Secondly, although ionospheric delays of a reference satellite could be absorbed by the receiver clock parameters (see Eqs. (13) and (14)), precise linear fitting and prediction of inter-satellite ionospheric delay require that the reference satellite should not have any large nonlinear temporal variations. Otherwise, it will introduce bias to other satellites. Hence, optimization of selection of reference satellite is absolutely necessary. Change of ionospheric slant delays is mainly caused by the change of the satellite elevation angle and by the change of the total electron content in space and time. As the latter is usually rather small and gentle over several minutes, we choose the satellite with the highest elevation angle as a reference satellite to minimize the effect of the change of elevation angle.

The stability of ionospheric delay of a satellite could be further assessed by the fitting residuals of the inter-satellite differenced ionospheric delays. Satellites with poor stability should be down weighed in order to reduce their bad effect on estimates.

Nevertheless, the predicted ionospheric delay for some satellites could still have large bias, although their polynomial fitting looks well. In order to get rid of such problematic predictions, a real-time quality control procedure is definitely necessary. We employed a very simple and commonly used method by checking the estimated observation residuals. At each epoch, we carried out the estimation with all observations. Then the problematic satellites are identified by checking the observation residuals and confirmed by their residuals estimated after discarding or down-weighting the observations of the related satellites.

Lastly, it should be pointed out that the linear model may be not so effective if there is nonlinear change in ionospheric delays, for example, under the equatorial ionospheric anomaly and scintillation. This is still an issue under investigation also for the method by Li et al. (2014a).

## 5. Outdoor validation and the application for 2011 Tohoku earthquake

Though assessing the performance of single-frequency GPS algorithm using L1 observations of dual-frequency receivers is a quite common practice among geodetic community (see, e.g., Van Bree and Tiberius, 2012; Tu et al., 2013; Li et al., 2014a), to demonstrate the reliability of single-frequency receiver, here the new method was evaluated first with a real single-frequency data of a dedicated experiment and then it was applied to the L1 observations

of dual-frequency receivers collected during the 2011 Tohoku earthquake.

### 5.1. Outdoor validation using a real single-frequency receiver

We first conducted an experiment using a real single-frequency NOVATEL (NOVATEL SmartAntenna in the OEM4 family) receiver. In addition, a dual-frequency JAVAD (JAVARD Delts- with an TRE-3 board and a Javad GrAnt G5T Antenna) receiver was also placed within one foot to the single-frequency receiver and they were fixed together by a piece of steel plate, the whole device for the test is shown in Fig. 1. By such a platform, the ionospheric delay of both receivers should be the same and their movements can be guaranteed to be strictly coherent .

Sampling rates of both receivers are 1 Hz, in order to obtain converged carrier phase ambiguities and precise receiver positions, we processed as long as 10 h JAVAD dual-frequency data using static PPP. After its position was determined, then position of NOVATEL was calculated in relative positioning mode with respect to the dual-frequency receiver. At last, the two receivers were pushed forward and backward for several times along the fixed track from 12, March, 2015,13:06 GPS time. Movements retrieved by dual-frequency TPP and our suggested method using single-frequency data are shown in Fig. 2. As clearly depicted, on horizontal direction, the performance of single-frequency is almost as good as dual-frequency, the RMS between them is at the level of 1.7 cm. For vertical component, it is slightly worse, the largest bias is almost 5 cm while the overall fit is limited to 3 cm in terms of RMS. To conclude, it is trustworthy to use the new method when it comes to single-frequency receiver.

Fig. 1. Experimental platform for single-frequency receiver validation.

### 5.2. Application for 2011 Tohoku earthquake

To validate the new method more broadly, we reprocessed 1 Hz GPS data collected by GEONET stations during the Great Mw 9.0 Tohoku earthquake (11 March, 2011, 05:46 UTC, GPS Time-UTC = 15s). Because original GPS data were actually collected in a dual-frequency mode, for their replay in a single-frequency scenario we used only C/A code and L1 phase. 75 stations across Japan were selected for data processing. Co-seismic displacements from dual-frequency TPP method was used for benchmark of the new method.

#### 5.2.1. Accuracy of predicted ionospheric change

As known, the geometry-free combination of dual-frequency data gives the ionospheric delay information according to:

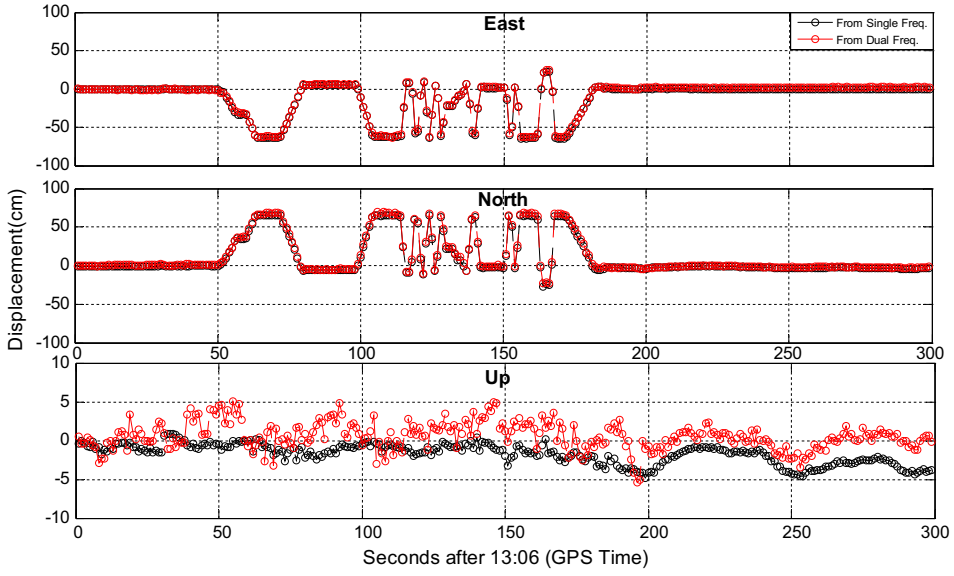


Fig. 2. Displacements retrieved from single-frequency and dual-frequency receiver.

$$LG = \lambda_1 \cdot L_1 - \lambda_2 \cdot L_2 = I \cdot c \cdot \frac{f_1^2 - f_2^2}{f_1^2 f_2^2} + (\lambda_1 \cdot N_1 - \lambda_2 \cdot N_2) \quad (16)$$

$I$ is the slant ionospheric delay, $c$, $f_i$, $\lambda_i$, $N_i$ are the speed of light, frequency, wavelength and phase ambiguity of the related signals, respectively.Assuming that there is no cycle slip from epoch $m$ to epoch $n$, the change of the delay on $L1$ can be expressed as:

$$I_{m,n} = LG_{m,n} \cdot \frac{f_2^2}{f_1^2 - f_2^2} \quad (17)$$

Since all the stations in the GEONET GPS-network are equipped with dual frequency receivers, such ionospheric delay changes could be derived as "ground truth" for evaluating the predicted ones.

In order to assess the accuracy of the predicted ionospheric delays and their impact on the estimated displacements, we selected observation window of about seven minutes length starting from the GPS-time 05:26, which is just 20 min prior to the main Tohoku 2011 shock. During this time window, GEONET stations experienced no notable displacements and their positions were well known.

First we computed the $L1$ residuals using Eq. (7) with known station coordinates for the whole period. Please note, since between-satellites single difference was adopted to remove the effect of receiver clock bias, residuals were then related to a reference satellite, so that they included mainly ionospheric delay changes and remaining errors in satellite orbits and clocks as well as residual tropospheric delays. The true ionospheric delay changes were also calculated with Eq. (17) using dual-frequency phase observations for comparison.

For illustration purpose, the residuals with respect to G27 and the true ionospheric changes at the station 0219 are shown in Fig. 3 together with satellite elevation angles.

One can see that ionospheric delay change is strongly correlated with both the absolute value and variations of the satellite elevation angle. For example, satellites G15 and G21 have very small change in elevation, as a result, their ionospheric delay changes do not exceed 10 cm. In contrast, ionospheric delay change of G18 reaches up to 65 cm. Note, despite G27 rises faster than G18, its ionospheric delay change is smaller because of the significantly higher elevation. As expected, G27'sionospheric delay change smoothly and nearly linearly supporting the feasibility of linear fitting.

Ionospheric delay changes from dual-frequency data were first converted to relative delay changes with respect to the same reference satellite G27 and then the differences between the two relative delay changes were calculated and shown in Fig. 4. They agree with each other better than 1 to 2 cm in RMS. This comparison verifies once again that the

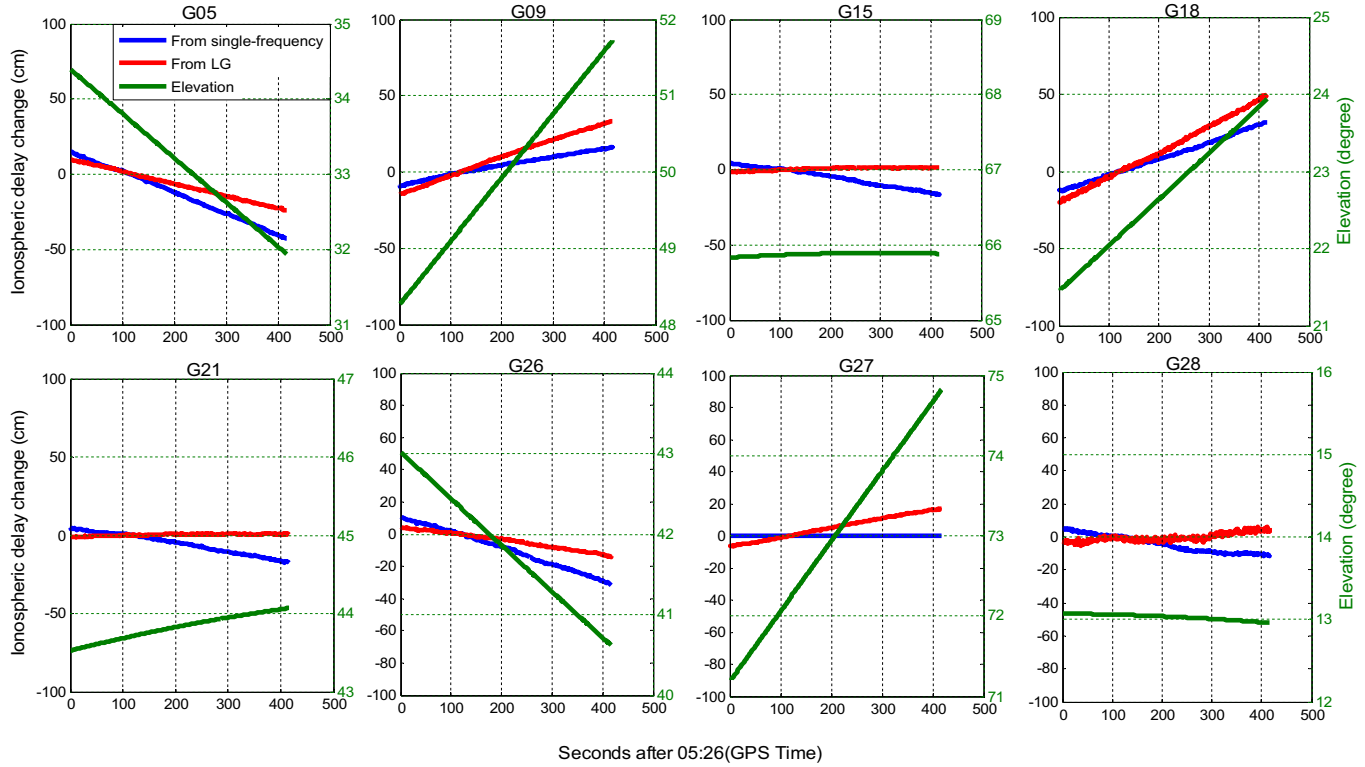


Fig. 3. Ionospheric delay changes on L1 frequency at station 0219: blue-derived with the proposed single-frequency method and using G27 as reference satellite; red-derived from dual-frequency observations. Elevation angles are also plotted (green). (For interpretation of the references to colour in this figure legend, the reader is referred to the web version of this article.)

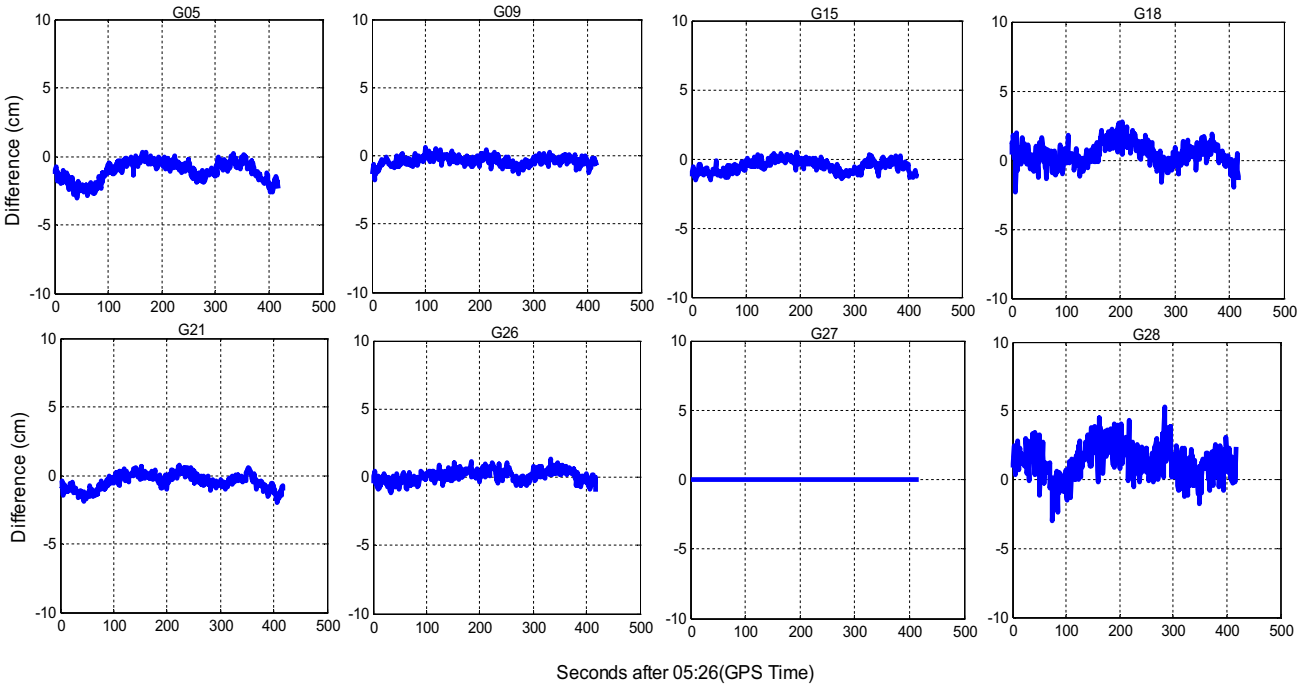


Fig. 4. Differences between relative ionospheric delay changes on L1 from single-frequency and from geometry-free combination of dual-frequency observations, here G27 is the reference satellite.

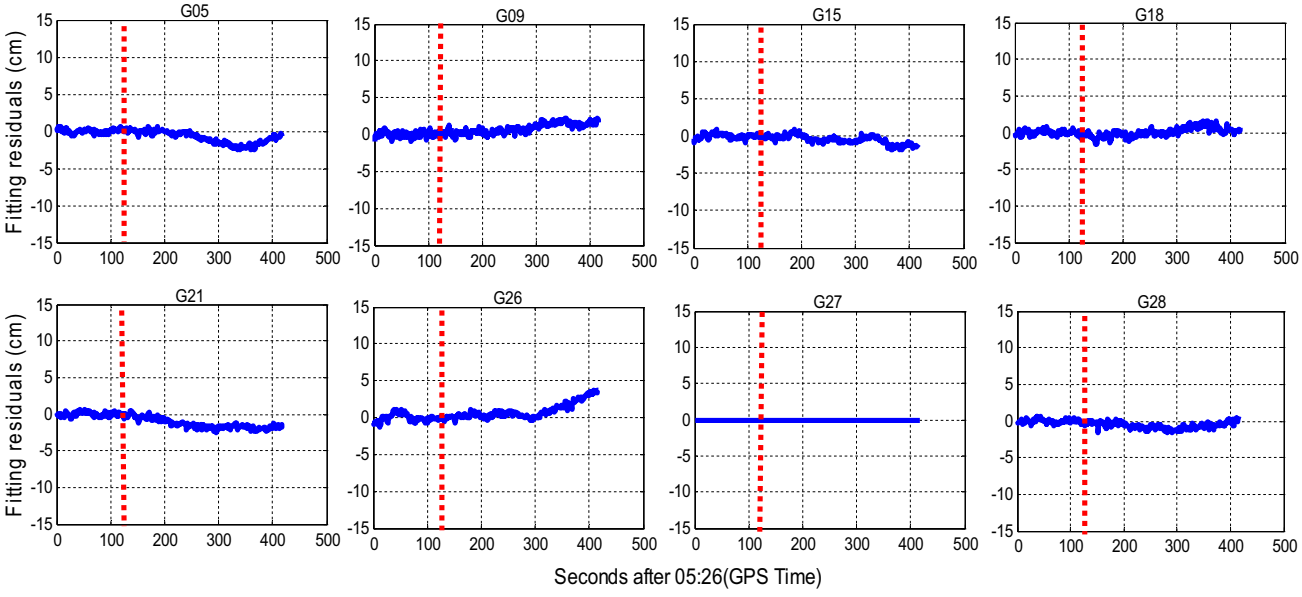


Fig. 5. Residuals of the L1 phase observations corrected by the predicted ionospheric delay changes based on two minutes data before the red dash line at station 0219, and G27 is reference satellite. (For interpretation of the references to color in this figure legend, the reader is referred to the web version of this article.)

new algorithm can represent relative ionospheric variations with enough degree of reliability.

Relative ionospheric delay changes during the first two minutes were used to establish a linear model for the ionospheric delay change of each satellite. With this estimated linear model, ionospheric delay changes for all epochs over next five minutes were calculated and applied to the observation equations. Pre-fit residuals shown in Fig. 5 can be considered as a quality index for the performance of the linear model. The red dashed line divides data into two parts: (1) two minutes before the dashed line for fitting and (2) five minutes for displacement estimation with predicted ionospheric corrections. Residuals of the first part can be also treated as residuals of the polynomial fitting.

For all satellites, the residuals are smaller than 1 cm RMS. This experiment convincingly demonstrates that within short time intervals, ionospheric delay changes can be fitted strictly linearly. Not surprisingly, error grows with time. However, on the whole, accuracy remains better than 2 cm.

Applying the corrections to the single-frequency data processing, we got the five-minute time series of displacements shown in Fig. 6. Variations in both horizontal and vertical components are limited to 2 cm and 3 cm, respectively.

For comparison, positioning was also performed using uncorrected L1 directly. As expected, the results (Fig. 7) show an obvious linear trend. Mostly, a linear fit model is suggested to remove this effect. Here we used the first two minutes time series to obtain the corresponding linear parameters. For east–west component, the model is quite encouraging. However, with respect to north–south and vertical components, the linear model causes tens of centimeters misfit, which implies linear fit cannot guarantee reliable accuracy.

### 5.2.2. Quality control of the predicted ionospheric delays

As mentioned above, there could be satellites with biased ionospheric delay predictions. This may result in contaminated displacement. Fig. 8 shows the displacement time series of station 0008 with an obvious drift of about

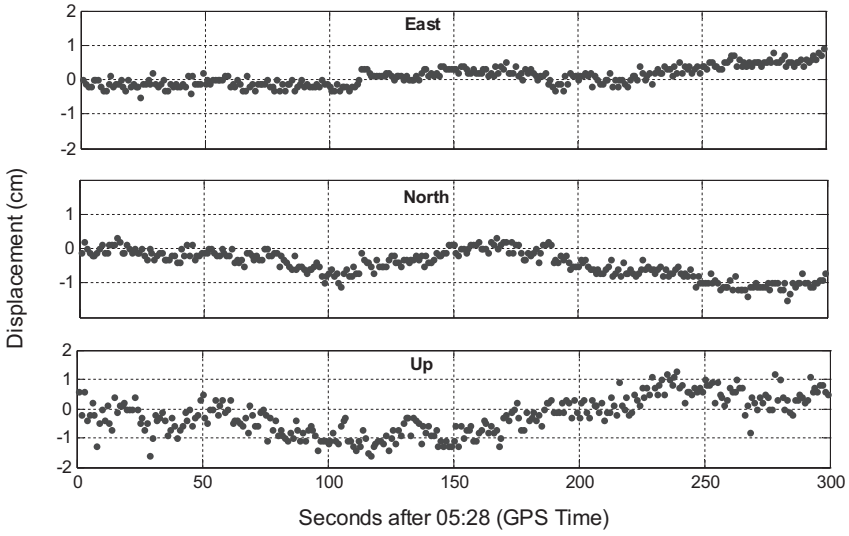


Fig. 6. Displacements of station 0219 using L1 phase observations, which were corrected by the predicted ionospheric delay changes.

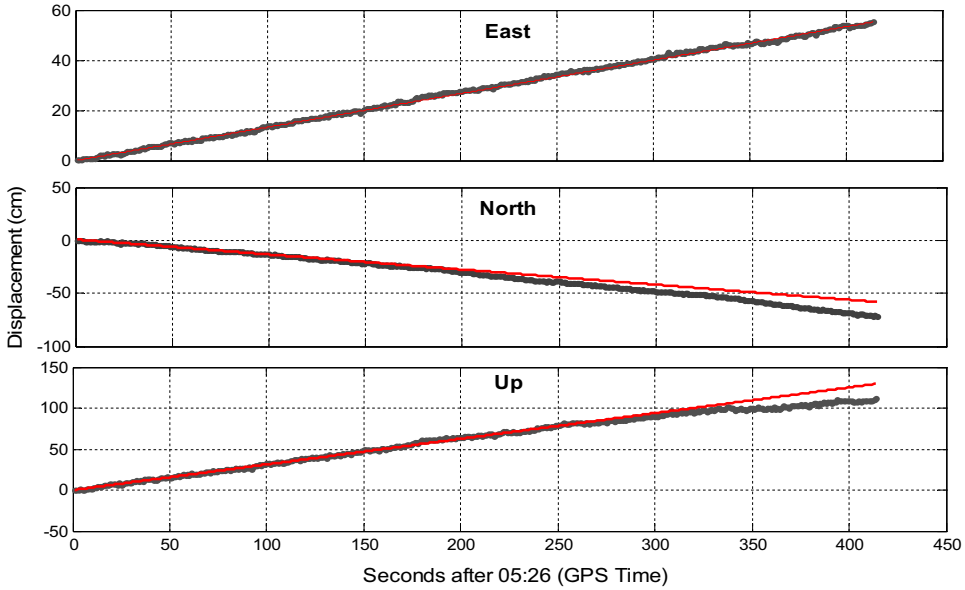


Fig. 7. Displacements of station 0219 using L1 phase observations without ionospheric delay correction, the black dots denote displacements while the red line means linear fit. (For interpretation of the references to color in this figure legend, the reader is referred to the web version of this article.)

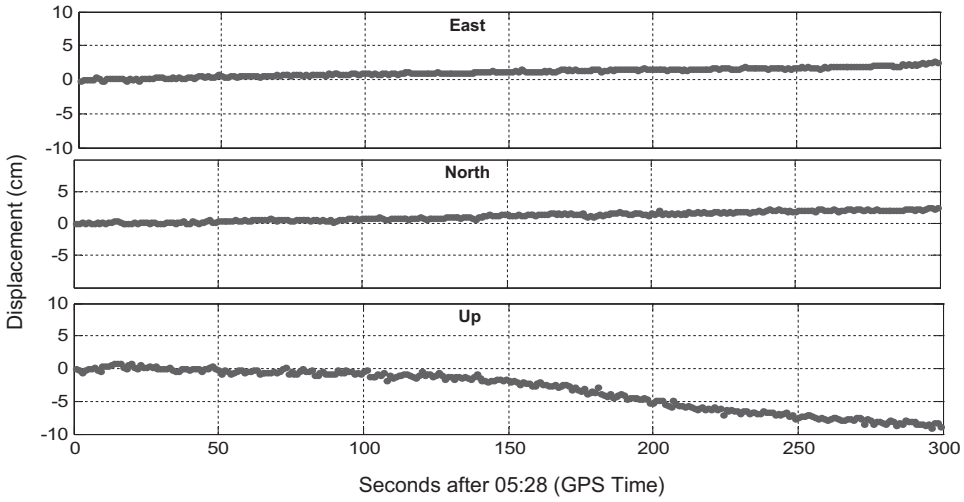


Fig. 8. Displacements of station 0008 (before quality control correction): an obvious drift exists in vertical component.

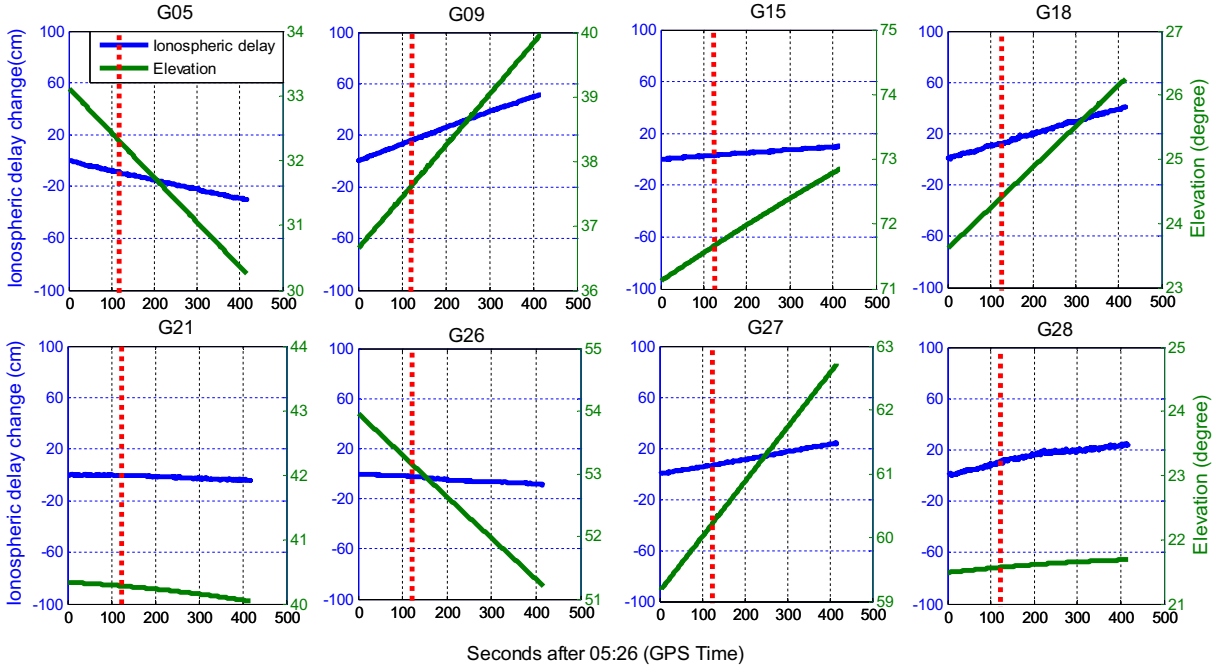


Fig. 9. Time evolution of the ionospheric delay (blue) and elevation angle change on L1 (green) at station 0008 starting from GPS Time 05:26. Time window from beginning to the red dash line is used to derive parameters for linear fitting. (For interpretation of the references to colour in this figure legend, the reader is referred to the web version of this article.)

10 cm in vertical component. As there was not any tectonic movement during the time period, the drift is most likely caused by a significantly wrong prediction of relative ionospheric delays. That is supported by the plot of ionospheric delays in Fig. 9. For satellite G28, the trend of ionospheric changes is very different for the time before and after the dashed line. In such a case, linear fitting produces a bias trend for the prediction interval. Note the large prediction error of about 13 cm for G28 in comparison with an error of a few centimeters for all other satellites (Fig. 10). Fortunately, bad predictions can be automatically detected by the proposed "quality control" procedure, so that displacements of high accuracy as shown in Fig. 11 could still be achieved. It should be pointed out, that there is a slight "jump" in the displacement time series after the problematic satellite is first detected and discarded. However, the typical "jump" is rather small (1 to 2 cm) and can be completely avoided by re-processing the original data without any detected problematic satellites.

### *5.2.3. Performance of single-frequency co-seismic displacements retrieving*

To guarantee that the approach used here was good during the moment of earthquake, we should first make sure

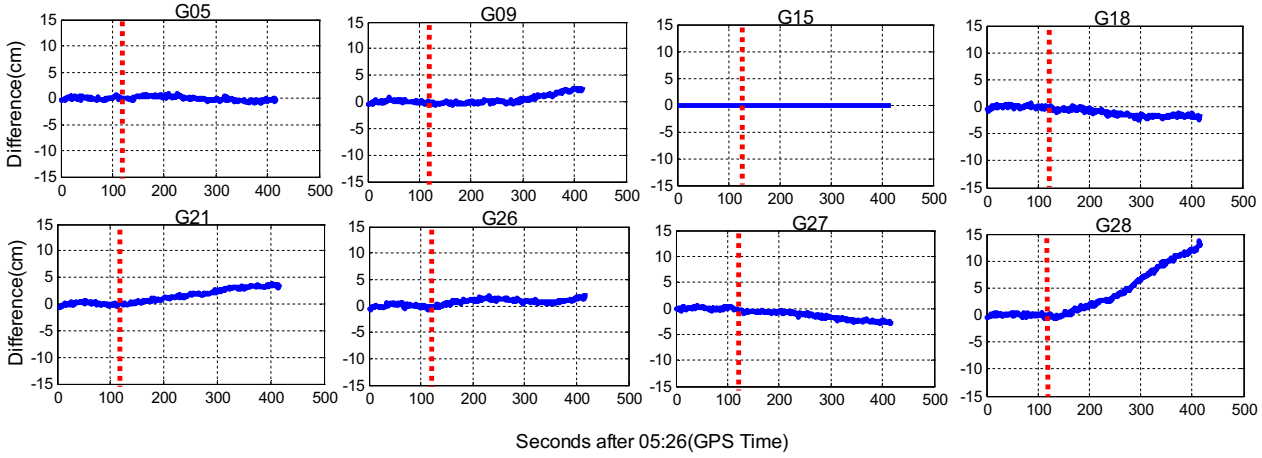


Fig. 10. L1 observation residuals at station 0008. Residuals before the dash line show precision of the linear fitting, while that after the dash line evidence about the quality of the predicted ionospheric delay changes.

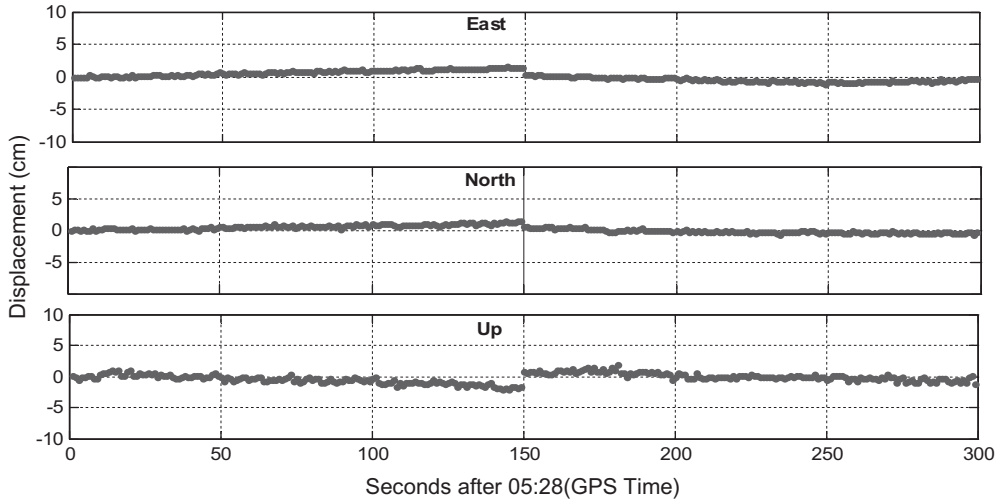


Fig. 11. Displacements at station 0008 after applying proposed quality control procedure. The jump shows the epoch from which the problematic predictions were detected and rejected.

that ionospheric delay at this time also changed linearly. Take station 0035 as an example, actual ionospheric delay derived from the dual-frequency data during shaking is then shown in Fig. 12, in which one can see ionospheric delay keeps linear. For data processing of each station, seven minutes of data stream were analyzed: first two minutes for polynomial fitting and the following five minutes for estimation of ground displacements. Displacements estimated by the two methods were compared, and the RMS of their differences over the five 'predicted' minutes was plotted on Fig. 13. In terms of the RMS, the horizontal and the vertical agreements are better than 2 cm for the whole period.

Fig. 14 shows co-seismic displacement waveforms at three selected GEONET stations derived with our new method for single-frequency data (blue line) and using the TPP method for dual-frequency data (red line). The three stations are located at different epicentral distances: station 0035 at 250 km; station 0046 at 560 km; and station 0066 at 850 km. Their co-seismic permanent displacements vary from about 2 meters to a few centimeters. Nevertheless, single-frequency displacement waveforms at all three stations are in very good agreement with the TPP displacement waveforms: discrepancies do not exceed a few centimeters during the whole evaluation period of 5 min. As can be expected, the discrepancy grows with time but remains within ±2.0 cm for horizontal and ±5 cm for vertical displacements, correspondingly.

Fig. 15 presents in map view the final static displacements corresponding to the main Tohoku 2011 shock. Static displacements at each station were obtained by averaging displacement waveforms over the last 20 s of the five minutes time period (refer to Fig. 14). It is vividly demonstrated that the static displacements derived by the two

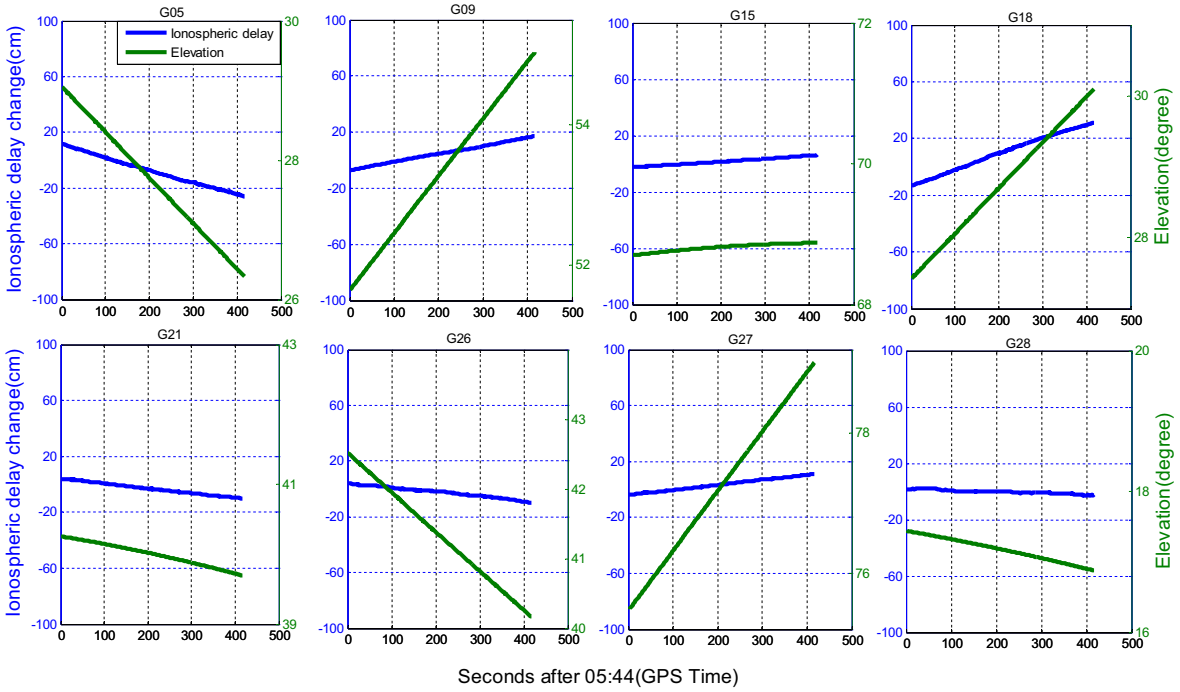


Fig. 12. Ionospheric delay change at station 0035 during earthquake time.

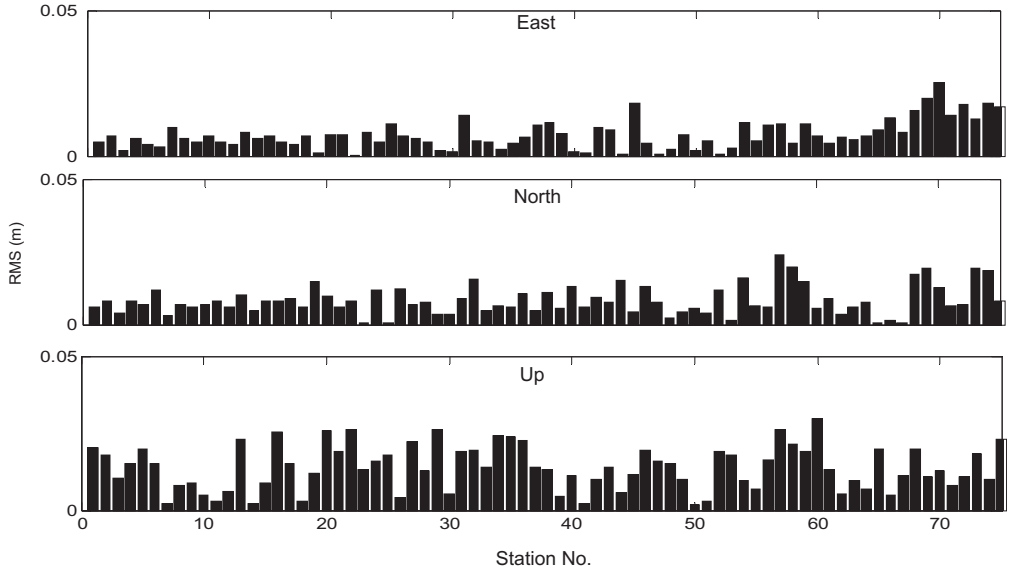


Fig. 13. RMS of the differences between co-seismic displacement waveforms derived by the new method and the traditional dual-frequency TPP method.

methods agree with each other very well. Corresponding differences for all 75 stations are shown in Fig. 16: RMS of the differences is 2 cm, 2 cm and 3 cm for east, north and vertical component, respectively. Furthermore, 10 h data before and after the earthquake broke were also processed by PPP static solution strategy and then static permanent displacements were computed by differencing. For convenience, here we name them as 'daily solution', which are also present in Fig. 15.This result clearly demonstrates that single-frequency data can be certainly employed for estimating co-seismic displacement for geohazard monitoring and early warning.

## 6. Conclusions and perspective

In this study, we have demonstrated the potential of using single-frequency GPS for retrieving co-seismic displacements in real-time. Use of inexpensive

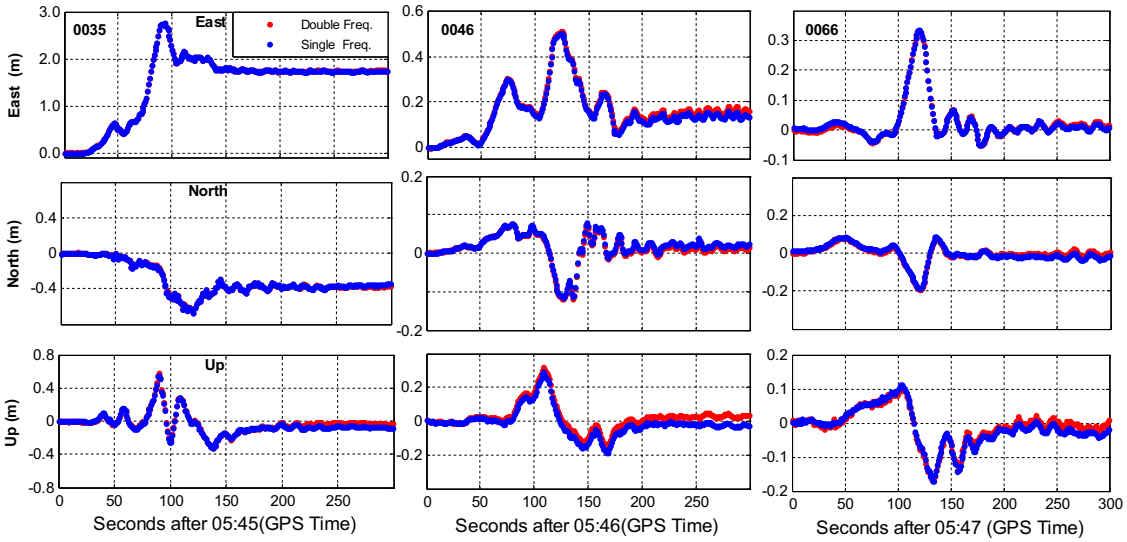


Fig. 14. Co-seismic displacement waveforms derived using the new single-frequency method compared to the traditional dual-frequency TPP method at three different GEONET GPS-network stations.

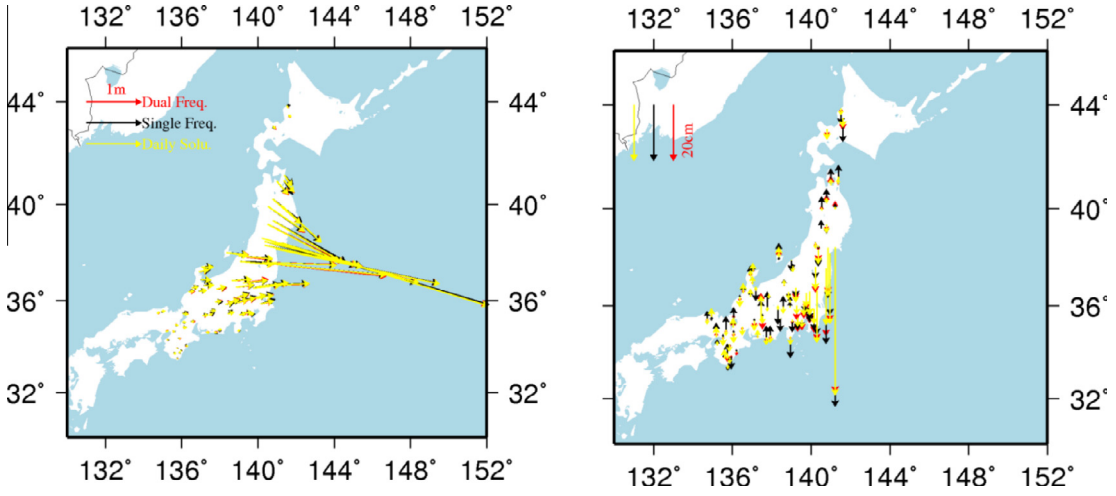


Fig. 15. Co-seismic static displacements due to Tohoku 2011 main shock derived by the new method using single-frequency data (black) and TPP using dual-frequency data (red). Left plot shows horizontal displacement, right-vertical displacement. (For interpretation of the references to colour in this figure legend, the reader is referred to the web version of this article.)

single-frequency GPS receivers may be economically favorable for the broad and dense geodetic networks required for earthquake and tsunami early warning. A new algorithm was developed based on the precise prediction of ionospheric delay changes over a short time window around the earthquake. A linear prediction model was selected to produce reliable results. We also suggest an automatic quality control procedure for detection and removal of problematic ionospheric corrections.

Accuracy of the new method was first tested by an outdoor experiment with simultaneous implication of single- and dual-frequency receivers. Average RMS constituted 1.7 cm for horizontal and 3 cm for the vertical component. We have also successfully validated our method by re-processing 1-Hz GPS data from the GEONET network during the 2011 Tohoku M9.0 earthquake. Kinematic and permanent co-seismic displacements obtained from the proposed method using single-frequency data was compared with that of the TPP method with dual-frequency data. Results evaluated at 75 GEONET stations show good agreement in terms of RMS: 2 cm, 2 cm, and 3 cm for east, north and vertical components, respectively. This work suggests that using single-frequency GPS receivers for monitoring and early warning of earthquake and related geohazards, e.g., tsunamis is feasible.

Considering the rapid development of multi-constellation-Global Navigation Satellite Systems (GNSSs) and more and more widely used multi-GNSSs

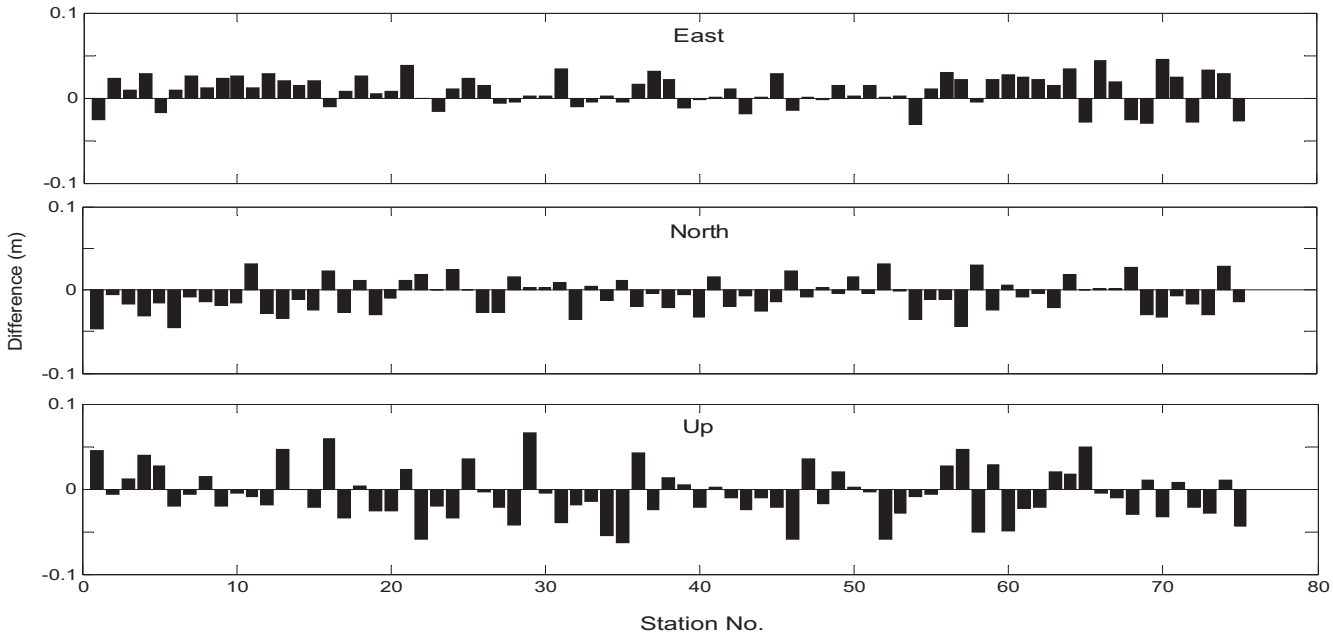


Fig. 16. Differences between co-seismic static displacements retrieved by the two methods at 75 GEONET stations (see description of Fig. 14).

receivers, the benefit of multi-GNSS (Li et al., 2015a,b) for geohazard applications will be investigated in the near future.

## Acknowledgments

Mr. Kejie Chen is financially supported by China Scholarship Council (CSC) for his PhD study at GFZ. 1 Hz GEONET GPS-network data were provided by the Geospatial Information Authority of Japan. This work are also supported by National Natural Science Foundation of China (Nos. 41231174 and 41474020). Three anonymous reviewers are acknowledged for their valuable comments which have improved this paper considerably.

## References

Benedetti, E., Branzanti, M., Biagi, L., Colosimo, G., Mazzoni, A., Crespi, M., 2014. Global navigation satellite systems seismology for the 2012 Mw 6.1 Emilia earthquake: exploiting the VADASE algorithm. Seismol. Res. Lett. 85 (3), 649–656.

Blewitt, G., Kreemer, C., Hammond, W.C., Plag, H.P., Stein, S., Okal, E., 2006. Rapid determination of earthquake magnitude using GPS for tsunami warning systems. Geophys. Res. Lett. 33 (11).

Boehm, J., Niell, A., Tregoning, P., Schuh, H., 2006. Global Mapping Function (GMF): a new empirical mapping function based on numerical weather model data. Geophys. Res. Lett. 33 (7).

Colosimo, G., Crespi, M., Mazzoni, A., 2011. Real-time GPS seismology with a stand-alone receiver: a preliminary feasibility demonstration. J. Geophys. Res.: Solid Earth 116 (B11) (1978–2012).

Geng, J., Meng, X., Dodson, A.H., Ge, M., Teferle, F.N., 2010. Rapid re-convergences to ambiguity-fixed solutions in precise point positioning. J. Geodesy 84 (12), 705–714.

Geng, J., Teferle, F.N., Meng, X., Dodson, A.H., 2011. Towards PPP-RTK: ambiguity resolution in real-time precise point positioning. Adv. Space Res. 47 (10), 1664–1673.

Geng, J., Bock, Y., Melgar, D., Crowell, B.W., Haase, J.S., 2013. A new seismogeodetic approach applied to GPS and accelerometer observations of the 2012 Brawley seismic swarm: Implications for earthquake early warning. Geochem. Geophys. Geosyst. 14 (7), 2124–2142.

Klobuchar, J.A., 1987. Ionospheric time-delay algorithm for single-frequency GPS users. IEEE Trans. Aerosp. Electron. Syst. 3, 325–331.

Larson, K.M., Bodin, P., Gomberg, J., 2003. Using 1-Hz GPS data to measure deformations caused by the Denali fault earthquake. Science 300 (5624), 1421–1424.

Lay, T., Kanamori, H., Ammon, C.J., Nettles, M., Ward, S.N., Aster, R.C., Beck, S.L., Bilek, S.L., Brudzinski, M.R., Butler, R., DeShon, H.R., Ekstrom, G., Satake, K., Sipkin, S., 2005. The great sumatra-andaman earthquake of 26 December 2004. Science 308, 1127–1133.

Li, X., Ge, M., Zhang, X., Zhang, Y., Guo, B., Wang, R., Wickert, J., 2013a. Real-time high-rate co-seismic displacement from ambiguity-fixed precise point positioning: Application to earthquake early warning. Geophys. Res. Lett. 40 (2), 295–300.

Li, X., Ge, M., Guo, B., Wickert, J., Schuh, H., 2013b. Temporal point positioning approach for real-time GNSS seismology using a single receiver. Geophys. Res. Lett. 40 (21), 5677–5682.

Li, M., Li, W., Fang, R., Shi, C., Zhao, Q., 2014a. Real-time high-precision earthquake monitoring using single-frequency GPS receivers. GPS Solutions 19 (1), 27–35.

Li, X., Guo, B., Lu, C., Ge, M., Wickert, J., Schuh, H., 2014b. Real-time GNSS seismology using a single receiver. Geophys. J. Int., ggu113

Li, X., Zhang, X., Ren, X., Fritsche, M., Wickert, J., Schuh, H., 2015a. Precise positioning with current multi-constellation Global Navigation Satellite Systems: GPS, GLONASS. Galileo and BeiDou. Sci Rep. 5, 8328.

Li, X., Ge, M., Dai, X., Ren, X., Fritsche, M., Wickert, J., Schuh, H., 2015b. Accuracy and reliability of multi-GNSS real-time precise positioning: GPS, GLONASS, BeiDou, and Galileo. J. Geodesy. http://dx.doi.org/10.1007/s00190-015-0802-8.

Lifton, Z.M., Newman, A.V., Frankel, K.L., Johnson, C.W., Dixon, T.H., 2013. Insights into distributed plate rates across the Walker Lane from GPS geodesy. Geophys. Res. Lett. 40 (17), 4620–4624.

Ohta, Y., Kobayashi, T., Tsushima, H., Miura, S., Hino, R., Takasu, T., Umino, N., 2012. Quasi real-time fault model estimation for near-field tsunami forecasting based on RTK-GPS analysis: Application to the 2011 Tohoku-Oki earthquake (Mw 9.0). J. Geophys. Res. Solid Earth 117 (B2) (1978–2012).

Prawirodirdjo, L., Bock, Y., 2004. Instantaneous global plate motion model from 12 years of continuous GPS observations. J. Geophys. Res. Solid Earth 109 (B8) (1978–2012).

Ren, J., Chen, G., Xu, X., Zhang, S., Mao, C., 2010. Surface rupture of the 2008 Wenchuan, China, earthquake in the Qingpingstepover determined from geomorphologic surveying and excavation, and its tectonic implications. Bull. Seismol. Soc. Am. 100 (5B), 2651–2659.

Saastamoinen, J., 1972. Atmospheric correction for the troposphere and stratosphere in radio ranging satellites. Geophys. Monograph Series 15, 247–251.

Schaer, S., Beutler, G., Rothacher, M., & Springer, T. A. (1996, March). Daily global ionosphere maps based on GPS carrier phase data routinely produced by the CODE Analysis Center. In Proceedings of the IGS AC Workshop, Silver Spring, MD, USA (pp. 181–192).

Schueler, T., 2014. The TropGrid2 standard tropospheric correction model. GPS Solutions 18 (1), 123–131.

Shi, C., Lou, Y., Zhang, H., Zhao, Q., Geng, J., Wang, R., Liu, J., 2010. Seismic deformation of the Mw 8.0 Wenchuan earthquake from high-rate GPS observations. Adv. Space Res. 46 (2), 228–235.

Sobolev, S.V., Babeyko, A.Y., Wang, R., Hoechner, A., Galas, R., Rothacher, M., Subarya, C., 2007. Tsunami early warning using GPS-Shield arrays. J. Geophys. Res. Solid Earth 112 (B8) (1978–2012).

Sudhakar, T., Suriyakala, C.D., Thangarasu, P., 2013. Case study of Tsunami warning system using RTK GPS method. In: Ocean Electronics (SYMPOL). IEEE, pp. 119–126.

Tu, R., Wang, R., Ge, M., Walter, T.R., Ramatschi, M., Milkereit, C., Dahm, T., 2013. Cost-effective monitoring of ground motion related to earthquakes, landslides, or volcanic activity by joint use of a single-frequency GPS and a MEMS accelerometer. Geophys. Res. Lett. 40 (15), 3825–3829.

Urquhart, L., Nievinski, F.G., Santos, M.C., 2014. Assessment of troposphere mapping functions using three-dimensional ray-tracing. GPS Solutions 18 (3), 345–354.

Van Bree, R.J., Tiberius, C.C., 2012. Real-time single-frequency precise point positioning: accuracy assessment. GPS Solutions 16 (2), 259–266.

Wang, Q., Zhang, P.Z., Freymueller, J.T., Bilham, R., Larson, K.M., Lai, X.A., Chen, Q., 2001. Present-day crustal deformation in China constrained by Global Positioning System measurements. Science 294 (5542), 574–577.

Zhang, X., Li, X., 2012. Instantaneous re-initialization in real-time kinematic ppp with cycle-slips fixing. GPS Solutions 16 (3), 315–327.